Research Article

Shuguang Li, Muhammad Nasir, Muhammad Waqas*, Shaimaa A. M. Abdelmohsen, Sayed M. Eldin, Sherzod Shukhratovich Abdullaev, and Waqar Azeem Khan

Bioconvection transport of upper convected Maxwell nanoliquid with gyrotactic microorganism, nonlinear thermal radiation, and chemical reaction

https://doi.org/10.1515/ntrev-2022-0569 received February 7, 2023; accepted June 20, 2023

Abstract: The microorganisms' concept has appealed substantial consideration of modern researchers because of its utilization in commercial and industrial products, for illustration, biofuel (prepared from the waste), drug delivery, and fertilizers. Keeping such utilizations of microorganisms in mind, an analysis based on gyrotactic microorganisms featuring the mixed convective nonlinear radiative Maxwell nanoliquid stagnation point flow configured by permeable stretching surface is presented. Boundary layer stretching flow subjected to transpiration effects is formulated. Modeling is based on Buongiorno's nanoliquid model. This model captures Brownian diffusion along with thermophoresis aspects. Energy expression is formulated under nonlinear version of radiative heat-flux, heat source, thermal Robin conditions, and heat sink. Mass transport

analysis is presented considering solutal Robin conditions and chemical reaction. In addition, the Robin conditions for motile microorganisms are also considered. The complex mathematical expressions of Maxwell liquid are simplified utilizing the Boundary layer concept and then suitable transformations assist to obtain the mathematical problems in ordinary differential forms. The analytical approach (that is homotopy analysis methodology) is utilized for computational analysis. The outcomes obtained are presented graphically and numerically. The detailed description of emerging physical non-dimensional parameters is included. Our findings indicate that the motile density field strongly boosted with the increment in Peclet number and microorganisms Biot number; however, they are suppressed with the increase in the values of bioconvection Schmidt number and motile microorganism concentration difference parameter.

Keywords: Maxwell nanoliquid, gyrotactic microorganisms, Brownian diffusion, Robin conditions, thermophoresis, chemical reaction, transpiration, nonlinear thermal radiation

* Corresponding author: Muhammad Waqas, NUTECH School of Applied Science and Humanities, National University of Technology, Islamabad 44000, Pakistan; Department of Mechanical Engineering, Lebanese American University, Beirut 1102, Lebanon, e-mail: mw_gau88@yahoo.com

Shuguang Li: School of Computer Science and Technology, Shandong Technology and Business University, Yantai 264005, China

Muhammad Nasir: Faculty of Informatics and Computing, Universiti Sultan Zainal Abidin, Besut Campus, 22200 Besut, Terengganu, Malaysia **Shaimaa A. M. Abdelmohsen:** Department of Physics, College of Science, Princess Nourah Bint Abdulrahman University, P.O. Box 84428, Riyadh, 11671, Saudi Arabia

Sayed M. Eldin: Center of Research, Faculty of Engineering, Future University in Egypt, New Cairo, 11835, Egypt

Sherzod Shukhratovich Abdullaev: Faculty of Chemical Engineering, New Uzbekistan University, Tashkent, Uzbekistan; Scientific Department, Tashkent State Pedagogical University named after Nizami, Tashkent, Uzbekistan

Waqar Azeem Khan: Department of Mathematics, Mohi-ud-Din Islamic University, Nerian Sharif, Azad Jammu & Kashmir, 12010, Pakistan

Nomenclature

A ratio of rates

 $C_{\rm f}$ heated fluid concentration

 C_{∞} ambient fluid concentration

 $D_{\rm t}$ thermophoretic diffusion coefficient (m² s⁻¹)

 $D_{\rm B}$ Brownian diffusion coefficient (m² s⁻¹)

f dimensionless velocity

Gr_x thermal buoyancy number

 Gr_x^* concentration buoyancy number

N thermophoresis parameter

*N** buoyancy ratio parameter

 $N_{\rm b}$ Brownian motion parameter

 $N_{\rm t}$ thermophoresis parameter

Nu_x local Nusselt number

2 — Shuguang Li et al. DE GRUYTER

10	Bioconvection reciet number
Pr	Prandtl number
R	radiation parameter
Rb	bioconvection Rayleigh number
Re_x	local Reynolds number
Sc_n	bioconvection Schmidt number
T	fluid temperature (K)
T_{∞}	ambient fluid temperature (K)
u, v	velocity components (m s ⁻¹)
<i>x</i> , <i>y</i>	coordinate axes (m)
$\theta_{ m R}$	temperature ratio parameter
Ω	concentration motile microorganisms' parameter
σ	chemical reaction parameter
η	similarity variable
γ_1	thermal Biot number
θ	dimensionless temperature
ϕ	volume fraction of nano-particles
$ ho_{ m f}$	density of base fluid (k gm ⁻³)
λ	mixed convection parameter
β	Deborah number
γ_3	motile microorganisms conjugate parameter
γ_2	solutal Biot number
ξ	dimensionless motile microorganisms

bioconvection Peclet number

1 Introduction

Pe

Owing to their exceptionally reliable rheological characteristics, non-Newtonian liquids have acquired remarkable attraction among engineers, scientists, and researchers. Their utilization in distinct biomedical, pharmaceutical, technological, and other disciplines of science is growing every day. Different models featuring non-Newtonian characteristics are suggested. The model considered here (Maxwell fluid) is the rate type non-Newtonian model which captures viscoelastic aspects in terms of stress relaxation time factor and this model has ample usage in mechanical engineering, computers, automobiles, polymer, and medical industries. Researchers considered this model under diverse physical aspects. For illustration, Hayat et al. [1] evaluated Maxwell liquid stagnation point laminar flow configured by moving convective surface. They employed homotopy analysis methodology (HAM) for computational outcomes. They noticed temperature reduction subjected to larger Prandtl number. Analysis of mixed convective Maxwell liquid based on Buongiorno's model was scrutinized by Nadeem et al. [2]. Their outcomes indicate increase in velocity when material parameter (Deborah number) is augmented. Megahed [3] analyzed variable properties effectiveness in magnetized Maxwell liquid incompressible flow under porous medium and Robin conditions. According to

his findings, larger Eckert number yields higher temperature. Transport of hybrid Maxwell nanoliquid considering buoyancy forces and improved Fourier–Fickian relations is reported by Madkhali *et al.* [4]. They declared that thermal memory aspects play vital contribution in augmenting the wall heat flux. Waqas [5] explored variable properties based on temperature and concentration in flow of chemically reactive Maxwell liquid laminar flow. It is examined that Prandtl number and heat sink factor corresponds to lower temperature when compared with variable conductivity and heat source parameters.

Nanoliquids upsurge the transportation of heat transfer utilized in intensification procedure of reactors and heat exchangers. Consideration of bioconvection in nanoliquids convalesce mass transportation, enhance stability, induce microvolume fraternization, and prevent nanoparticles clustering [6,7]. The nanoliquids together with bioconvection aspect find relevance in medical filtration, microfluidic devices, microbial fuel cells, modernized energy conservation mechanisms, and bio-nano coolant structures. The gyrotactic microorganisms significance in nanoliquid stagnant point flow is evaluated by Zaimi et al. [8]. Xu and Pop [9] modeled the mixed convective gyrotactic microorganisms based nanoliquid flow employing homotopic scheme. Their outcomes signify concentration augmentation subject to increasing thermophoresis variable. Magnetohydrodynamic laminar flow based on Oldroyd-B model capturing Buongiorno's nanoliquid and stratifications was inspected by Wagas et al. [10]. It is noticed that higher Peclet number yields diminution of microorganisms' density. Further analyses featuring gyrotactic microorganisms in stretching flow of rheological liquids are mentioned in previous studies [11–13]. In these investigations, multi-physical effects along with distinct geometries are considered. From these studies, it is concluded that nanoliquid consideration together with gyrotactic microorganisms stabilize the adjourned nanoparticles.

Undoubtedly, numerous engineering and geological structures capturing double-diffusive convection effects encompass the phenomenon of chemical reaction. Geochemical flows involve rainfall reaction (for example a calcium feldspar and acidic brine), pollutant leaching [14], mineralogical dissolution, and brine chemo-geothermics [15]. Further examples based on industrial technologies comprise catalytic conversion, manipulation of polymer radical, materials synthesis [16], and exothermic type chemical reactions featuring porous media based reactors [17]. Rheological liquid models subjected to chemical reactions are scrutinized by various researchers considering multi-physical effects and geometries. In this direction, Reddy *et al.* [18] examined chemically reactive magnetized laminar flow subjected to porous medium and viscous dissipation. They considered micropolar model

for flow formulation. They inspected higher thermal field for increasing radiation factor and Eckert number. Chemically reactive Eyring-Powell liquid incompressible stretching flow confined by heated convective surface is scrutinized by Hussain et al. [19]. They computed nonlinear problems using byp4c algorithm. They found significant impact of chemical reaction factor on mass transportation. Chu et al. [20] evaluated Maxwell nanoliquid stagnation point reactive flow considering cylindrical geometry. They declared that consideration of exponential heat source together with nonlinear radiation is significant when improvement in thermal processes is required.

The literature mentioned above witness that Darcy-Forchheimer concept of porous medium in rate type stretching liquids subjected to gyrotactic microorganisms is less considered. With this objective, our focus here is to develop a mathematical model featuring nonlinear rheological Maxwell liquid. The current study accounts the novel aspects like thermal radiation, stagnant point flow, chemical reaction, and Robin conditions. The boundary layer approach yielding parabolic expressions is used. Various computational algorithms [21–24] are available. Here the governing mathematical problems of Maxwell liquid are analytically solved through HAM [25-28]. The outcomes of significant variables against dimensionless quantities are presented and elaborated comprehensively. The considered non-Newtonian nanoliquid stagnation model encompasses coating fabricating procedures for biomimetic sensors [29] and optical fiber nano-coatings [30,31].

2 Flow model

Consider a laminar boundary layer stretching flow based on rate type rheological Maxwell liquid [26] confined by vertical convective permeable surface. Stagnation point incompressible flow is modeled in vertical direction considering buoyancy forces and velocity $u_w(x) = cx$. The Maxwell nanoliquid is electrically conductive and is exposed to a uniform magnetic field B_0 . The dispersion of nanoparticles is homogeneous, which prevents agglomeration and accumulation, resulting in a dilute nanofluid suspension. In addition, the model assumes that the swimming direction and velocity of gyrotactic microorganisms are not impacted by nanoparticles presence. The density variation in buoyancy term is determined utilizing the Boussinesq approximation. The flow configuration is illustrated in Figure 1.

The governing nonlinear expressions subjected to mixed convection, gyrotactic microorganisms, thermal radiation, Robin conditions, and heat source/sink are as follows [27]:

$$\frac{\partial u}{\partial x} + \frac{\partial v}{\partial y} = 0, \tag{1}$$

$$u \frac{\partial u}{\partial x} + v \frac{\partial u}{\partial y} + \lambda_1 \left[u^2 \frac{\partial^2 u}{\partial x^2} + v^2 \frac{\partial^2 v}{\partial y^2} + 2uv \frac{\partial^2 u}{\partial x \partial y} \right]$$

$$= v \frac{\partial^2 u}{\partial y^2} + u_e \frac{du_e}{dx} + \frac{1}{\rho_f} [(1 - C_\infty) \rho_f g \beta (T - T_\infty)$$

$$- (\rho_v - \rho_f) g (C - C_\infty) - (\rho_m - \rho_f) g \gamma (n - n_\infty)],$$

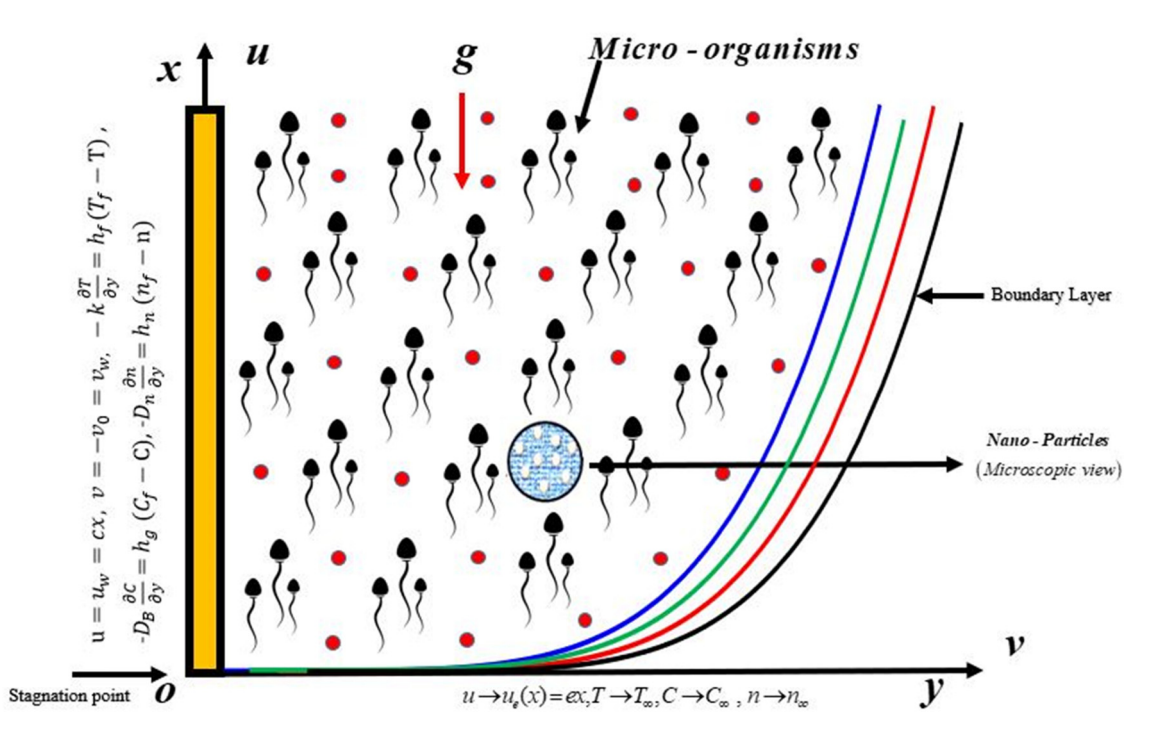


Figure 1: Flow diagram and coordinate system.

4 — Shuguang Li et al. DE GRUYTER

$$u\frac{\partial T}{\partial x} + v\frac{\partial T}{\partial y} = \alpha \frac{\partial^{2} T}{\partial y^{2}} + \tau \left[D_{\rm B} \frac{\partial C}{\partial y} \frac{\partial T}{\partial y} + \frac{D_{\rm T}}{T_{\infty}} \left(\frac{\partial T}{\partial y} \right)^{2} \right] + \frac{16\sigma^{*}}{3k^{*}(\rho c)_{\rm f}} \frac{\partial}{\partial y} \left[T^{3} \frac{\partial T}{\partial y} \right] + \frac{Q_{0}}{(\rho c)_{\rm f}} (T - T_{\infty}),$$
(3)

$$u\frac{\partial C}{\partial x} + v\frac{\partial C}{\partial y} = D_{\rm B}\frac{\partial^2 C}{\partial y^2} + \frac{D_{\rm T}}{T_{\infty}}\frac{\partial^2 T}{\partial y^2} - k_{\rm r}(C - C_{\infty}), \quad (4)$$

$$u\frac{\partial n}{\partial x} + v\frac{\partial n}{\partial y} + \frac{bW_{\rm c}}{(C_{\rm w} - C_{\infty})} \left[\frac{\partial}{\partial y} \left[n\frac{\partial C}{\partial y} \right] \right] = D_{\rm n} \left(\frac{\partial^2 n}{\partial y^2} \right), \quad (5)$$

$$u = u_{w}(x) = cx, v = v_{w} = -v_{0}, -k\frac{\partial T}{\partial y} = h_{f}(T_{f} - T),$$

$$-D_{\rm B}\frac{\partial C}{\partial y} = h_{\rm g}(C_{\rm f} - C), -D_{\rm n}\frac{\partial n}{\partial y} = h_{\rm n}(n_{\rm f} - n) \text{ at } y = 0,$$

$$u \to u_{\rm e}(x) = ex, T \to T_{\infty}, C \to C_{\infty}, n \to n_{\infty} \text{ when } y \to \infty,$$

where $v\!\!\left(\!=\!\!\frac{\mu}{\rho_{\mathrm{f}}}\!\right)$ represents the kinematic viscosity, ρ_{f} repre-

sents the liquid density, μ denotes the dynamic viscosity, Q_0 stands for the heat absorption (sink)/generation (source) coefficient, γ is the average volume of microorganisms, $ho_{
m p}$ and $ho_{
m m}$ stand for the particle microorganisms densities, $(u_{\rm w}(x), v_{\rm w})$ stand for the (stretching, suction/injection) velocity, λ_1 is the relaxation time, g is the gravitational acceleration, $D_{\rm B}$ is the Brownian diffusion coefficient, b is the chemotaxis constant, W_c is the maximum cell swimming speed, Dn is the microorganisms diffusion coefficients, C is the liquid concentration, $u_e(x)$ is free stream velocity, $C_{\rm f}$ is the heated liquid concentration, thermal diffusivity $\alpha = \frac{k}{(\rho c)_f}$, heat capacity ratio $\tau = \frac{(\rho c)_P}{(\rho c)_f}$ with liquid heat $(\rho c)_{\rm f}$, $(\rho c)_{\rm p}$ stands for the nanoparticles effective heat capacity, $(h_{\rm f},h_{\rm g},h_{\rm n})$ stand for the heat, mass, and motile microorganisms transfer coefficients, σ^* is the Stefan–Boltzmann constant, D_T is the thermophoresis diffusion coefficient, C_{∞} is the ambient liquid concentration, k^* is the mean absorption coefficient, *n* is the motile microorganisms concentration, *T* is the liquid temperature, T_f is the heated liquid temperature, kis the thermal conductivity, c is the dimensional constant, k_r is the reaction rate, T_{∞} is ambient liquid temperature, $n_{\rm f}$ is the microorganisms transfer coefficient, b is the chemotaxis constant, and u, v are the components of velocity in the (x, y)direction, respectively.

Implementing [27]

$$\begin{cases} \eta = y\sqrt{\frac{c}{v}}, \ u = cxf'(\eta), \ v = -\sqrt{cv}f(\eta), \\ \theta(\eta) = \frac{T - T_{\infty}}{T_{\rm f} - T_{\infty}}, \phi(\eta) = \frac{C - C_{\infty}}{C_{\rm f} - C_{\infty}}, \xi(\eta) = \frac{n - n_{\infty}}{n_{\rm f} - n_{\infty}}, \end{cases}$$
(7)

continuity equation (that is equation (1)) is fulfilled and other equations in dimensionless form become

$$f''' + f f'' + \beta(2f f' f'' - f^2 f''') - f'^2 + \lambda(\theta - N^*\phi - Rb\xi) + A^2 = 0,$$
(8)

$$(1 + R)\theta'' + \frac{4}{3}R[(\theta_R - 1)^3(3\theta^2(\theta')^2 + \theta^3\theta'') + 3(\theta_R - 1)^2(2\theta(\theta')^2 + \theta^2\theta'') + 3(\theta_R - 1)((\theta')^2 + \theta\theta'')]$$

$$+ \Pr(\theta') + \Pr(\theta')^2 + Nb\phi'\theta' + S\theta) = 0,$$
(9)

$$\phi'' + \operatorname{Sc} f \phi' + \frac{Nt}{Nh} \theta'' - \operatorname{Sc} \sigma \phi = 0, \tag{10}$$

$$\xi'' + Sc_n f \xi' - Pe[\xi' \phi' + (\xi + \Omega) \phi''] = 0,$$
 (11)

$$f = h, f' = 1, \theta' = -\gamma_1 (1 - \theta(\eta))$$

$$\phi' = -\gamma_2 (1 - \phi(\eta)), \ \xi' = -\gamma_2 (1 - \xi(\eta)) \text{ at } \eta = 0,$$
 (12)

$$f' \to A, \theta \to 0, \phi \to 0, \xi \to 0 \text{ as } \eta \to \infty,$$
 (13)

where (') signifies the differentiation concerning η , λ is the mixed convection parameter, Sc is the Schmidt number, Sc_n is the bioconvection Schmidt number, S < 0 is the heat absorption variable, Rb is the bioconvection Rayleigh number, Gr_x^* is the concentration buoyancy number, A is the ratio of rates, Nt is the thermophoresis parameter, Pr is the Prandtl number, Gr_x is the thermal buoyancy number, Nb is the Brownian motion parameter, R is the radiation variable, S > 0 is the heat generation variable, θ_R is the temperature ratio parameter, γ_1 is the thermal Biot number, β is the Deborah number, N^* is the buoyancy ratio parameter.

meter, $\sigma = \left(\frac{k_r^2}{c}\right)$ is the dimensionless reaction rate, γ_3 is the motile microorganisms conjugate parameter, $\sigma > 0$ is the destructive reaction variable, Ω is the concentration motile microorganisms parameter, Pe is the bioconvection Peclet number, $\sigma < 0$ is the generative reaction variable, γ_2 is the concentration Biot number, γ_2 is the suction, and γ_2 is the injection. These parameters are defined as follows:

$$\beta = \lambda_{1}c, \ \lambda = \frac{(1 - C_{\infty})\beta g(T_{f} - T_{\infty})}{c^{2}x},$$

$$Re_{x} = \frac{xu_{w}}{v}, Pr = \frac{v}{\alpha}, \gamma_{3} = h_{n}\sqrt{\frac{v}{c}},$$

$$N^{*} = \frac{(\rho_{p} - \rho_{f})(C_{f} - C_{\infty})}{\rho_{f}\beta(T_{f} - T_{\infty})(1 - C_{\infty})}, Nt = \frac{\tau D_{T}(T_{f} - T_{\infty})}{T_{\infty}\alpha},$$

$$Rb = \frac{r(n_{f} - n_{\infty})(\rho_{m} - \rho_{f})}{\beta \rho_{f}(1 - C_{\infty})(T_{f} - T_{\infty})}, S = \frac{Q_{0}}{(\rho c)_{f}c},$$

$$Sc = \frac{v}{D_{B}}, Sc_{n} = \frac{v}{D_{n}}, Pe = \frac{bW_{c}}{D_{n}}, \gamma_{1} = \frac{h_{f}}{k}\sqrt{\frac{v}{c}},$$

$$Nb = \frac{\tau D_{B}(C_{f} - C_{\infty})}{\alpha}, A = \frac{e}{c}, \theta_{R} = \frac{T_{f}}{T_{\infty}},$$

$$h = \frac{-v_{0}}{\sqrt{vc}},$$

$$\gamma_{2} = \frac{h_{g}}{D_{B}}\sqrt{\frac{v}{c}}, \sigma = \left(\frac{k_{r}^{2}}{c}\right), \Omega = \frac{n_{\infty}}{n_{f} - n_{\infty}}.$$
(14)

Heat-mass transportation and microorganism diffusion rates (Nu_x , Sh_x , Nn_x) in mathematical forms are defined as follows:

$$Nu_{x} = \left[-\frac{x}{(T_{f} - T_{\infty})} \left(\frac{\partial T}{\partial y} \right) - \frac{16\sigma^{*}x}{3kk^{*}(T_{f} - T_{\infty})} T^{3} \frac{\partial T}{\partial y} \right]_{y=0}, (15)$$

$$Sh_{x} = \frac{xq_{m}}{D_{B}(C_{f} - C_{\infty})}, \ q_{m} = -D_{B}\left(\frac{\partial C}{\partial y}\right)_{y=0}, \tag{16}$$

$$Nn_{x} = \frac{xq_{n}}{D_{n}(n_{f} - n_{\infty})}, q_{n} = \left(-D_{n}\frac{\partial \xi}{\partial y}\right)_{y=0},$$
(17)

$$Nu_{X}Re_{X}^{-0.5} = -\left(1 + \frac{4}{3}R(1 + (\theta_{R} - 1)\theta(0))^{3}\right)\theta'(0), \quad (18)$$

$$\operatorname{Sh}_{x} \operatorname{Re}_{x}^{-\frac{1}{2}} = -\phi'(0),$$

 $\operatorname{Nn}_{x} \operatorname{Re}_{x}^{-1/2} = -\xi'(0).$ (19)

3 Analytical solution procedure

In numerous engineering and industrial applications, the resultant coupled ordinary differential equations are extremely nonlinear, which is always a difficult task for engineers and researchers. Such difficult problems are frequently addressed either analytically or numerically. Beyond the analytical approaches, HAM approach is one that efficiently calculates the required convergence series solution of the system. One of the prominent features of this approach is

that it does not impose the restriction of big or small parameter in the problem. The convergence domain associated with this approach can be managed more effectively as related to other methodologies. It provides a lot of flexibility to build the necessary functions to calculate the solution. Liao [25] initiated the pioneering study on this approach. Later on, several researchers used this approach to solve highly nonlinear problems [26–28]. Following initial estimations, $(f_o(\eta), \theta_o(\eta), \phi_o(\eta), \xi_o(\eta))$ are proposed to start the computations.

$$f_{0}(\eta) = h + A*\eta + (1 - A)(1 - e^{-\eta}),$$

$$\theta_{0}(\eta) = \left(\frac{\gamma_{1}}{1 + \gamma_{1}}\right) *e^{-\eta},$$

$$\phi_{0}(\eta) = \left(\frac{\gamma_{2}}{1 + \gamma_{2}}\right) *e^{-\eta},$$

$$\xi_{0}(\eta) = \left(\frac{\gamma_{3}}{1 + \gamma_{3}}\right) *e^{-\eta}.$$
(20)

Let us assume the essential linear operators $(L_f,\ L_\theta,\ L_f,L_\xi)$ as follows:

$$\begin{cases}
L_f = f''' - f', \\
L_\theta = \theta'' - \theta, \\
L_\phi = \phi'' - \phi, \\
L_\xi = \xi'' - \xi.
\end{cases}$$
(21)

with

$$\begin{cases} L_{f}(A_{1} + A_{2}e^{\eta} + A_{3}e^{-\eta}) = 0, \\ L_{\theta}(A_{4}e^{\eta} + A_{5}e^{-\eta}) = 0, \\ L_{\phi}(A_{6}e^{\eta} + A_{7}e^{-\eta}) = 0, \\ L_{\xi}(A_{8}e^{\eta} + A_{9}e^{-\eta}) = 0, \end{cases}$$
(22)

where $A_i(i = 1 - 9)$ indicate the arbitrary constants. Now defining the problems at zeroth order, we have

$$(1 - w^*)L_f[\hat{f}(\eta; w^*) - f_0(\eta)] = w^*\hbar_f \mathbf{N}_f[\hat{f}(\eta; w^*), \\ \hat{\theta}(\eta, w^*), \ \hat{\phi}(\eta; w^*), \ \hat{\xi}(\eta; w^*)],$$
(23)

$$(1 - w^*)L_{\theta}[\hat{\theta}(\eta; w^*) - \theta_0(\eta)] = w^*\hbar_{\theta}\mathbf{N}_{\theta}[\hat{f}(\eta; w^*), \\ \hat{\theta}(\eta, w^*), \hat{\phi}(\eta; w^*), \hat{\xi}(\eta; w^*)],$$
(24)

$$(1 - w^*) L_{\varphi}[\hat{\phi}(\eta; w^*) - \phi_0(\eta)] = w^* \hbar_{\phi} \mathbf{N}_{\phi}[\hat{f}(\eta; w^*), \\ \hat{\theta}(\eta, w^*), \hat{\phi}(\eta; w^*), \hat{\xi}(\eta; w^*)],$$
(25)

$$(1 - w^*) L_{\xi}[\hat{\xi}(\eta; w^*) - \xi_0(\eta)] = w^* \hbar_{\xi} \mathbf{N}_{\xi}[\hat{f}(\eta; w^*), \\ \hat{\theta}(\eta, w^*), \hat{\phi}(\eta; w^*), \hat{\xi}(\eta; w^*)],$$
(26)

6 — Shuquang Li et al. DE GRUYTER

(28)

(29)

(30)

$$\begin{split} \hat{f}(0;\,w^*) &= h,\, \hat{f}'(0;\,w^*) = 1,\, \hat{f}'(\infty;\,w^*) = \,A,\\ \hat{\theta}'(0;\,w^*) &= -\gamma_1(1-\hat{\theta}(0;\,w^*)),\,\, \hat{\theta}(\infty;\,w^*) = 0,\\ \hat{\phi}'(0;\,w^*) &= -\gamma_2(1-\hat{\phi}(0;\,w^*)),\,\, \hat{\phi}(\infty;\,w^*) = 0,\\ \hat{\xi}(0;\,w^*) &= -\gamma_3(1-\hat{\xi}(0;\,w^*)),\,\, \hat{\xi}(\infty;\,w^*) = 0, \end{split}$$

$$\begin{split} \mathbf{N}_{f} [\hat{f}(\eta; \, w^{*}), \hat{\theta}(\eta; \, w^{*}), \hat{\phi}(\eta; \, w^{*}), \hat{\xi}(\eta; \, w^{*})] \\ &= \frac{\partial^{3} \hat{f}(\eta; \, w^{*})}{\partial \eta^{3}} + (\hat{f}(\eta, \, \, w^{*}) \frac{\partial^{2} \hat{f}(\eta; \, w^{*})}{\partial \eta^{2}} - \left[\frac{\partial \hat{f}(\eta; \, w^{*})}{\partial \eta} \right]^{2} \\ &+ \beta \left[2 \hat{f}(\eta, \, \, w^{*}) \frac{\partial \hat{f}(\eta; \, w^{*})}{\partial \eta} \frac{\partial^{2} \hat{f}(\eta; \, w^{*})}{\partial \eta^{2}} \right. \\ &- ((\hat{f}(\eta, \, \, w^{*}))^{2} \frac{\partial^{3} \hat{f}(\eta; \, w^{*})}{\partial \eta^{3}} \right] + 2\lambda(\hat{\theta}(\eta; \, w^{*}) \\ &- N^{*} \hat{\phi}(\eta; \, w^{*}) - \text{Rb} \hat{\xi}(\eta; \, w^{*})) + A^{2}, \end{split}$$

$$\begin{split} \mathbf{N}_{\varphi} [\hat{f}(\eta; w^*), \ \hat{\theta}(\eta; w^*), \ \hat{\phi}(\eta; w^*), \ \hat{\xi}(\eta; w^*)] \\ &= \frac{\partial^2 \hat{\phi}(\eta; w^*)}{\partial \eta^2} + \mathrm{Sc}\hat{f}(\eta; w^*) \frac{\partial \hat{\phi}(\eta; w^*)}{\partial \eta} \\ &+ \frac{N_{\mathrm{t}}}{N_{\mathrm{b}}} \frac{\partial^2 \hat{\theta}(\eta; w^*)}{\partial \eta^2} - \mathrm{Sc}\sigma\hat{\phi}(\eta; w^*), \end{split}$$

(27)
$$N_{\xi}[\hat{f}(\eta; w^*), \ \hat{\theta}(\eta; w^*), \ \hat{\phi}(\eta; w^*), \ \hat{\xi}(\eta; w^*)] = \frac{\partial^2 \hat{\xi}(\eta; w^*)}{\partial \eta^2} + \operatorname{Sc}_n \hat{f}(\eta; w^*) \frac{\partial \hat{\xi}(\eta; w^*)}{\partial \eta} - \operatorname{Pe}\left[\frac{\partial \hat{\xi}(\eta; w^*)}{\partial \eta} \frac{\partial \hat{\phi}(\eta; w^*)}{\partial \eta} + (\hat{\xi}(\eta; w^*) + \Omega) \frac{\partial^2 \hat{\phi}(\eta; w^*)}{\partial \eta^2}\right].$$

The embedding variable is shown by w^* while \hbar_f , \hbar_θ , \hbar_ϕ , and \hbar_ξ are non-zero auxiliary variables.

4 Convergence analysis of HAM

The analytical scheme known as HAM is deployed for computational outcomes. It comprises the auxiliary factors \hbar_f , \hbar_θ , \hbar_ϕ , and \hbar_ξ which assist in controlling convergence of homotopy solutions. Here the \hbar -curves for velocity distribution f''(0), temperature distribution $\theta'(0)$, concentration distribution $\phi'(0)$, and motile density distribution $\xi'(0)$ are depicted for particular values of prominent parameters in Figures 2 and 3. These figures witness that \hbar_f , \hbar_θ , \hbar_ϕ , and \hbar_ξ lie in $-1.3 \leq h_f \leq -0.4$, $-1.2 \leq h_\theta \leq -0.6$,

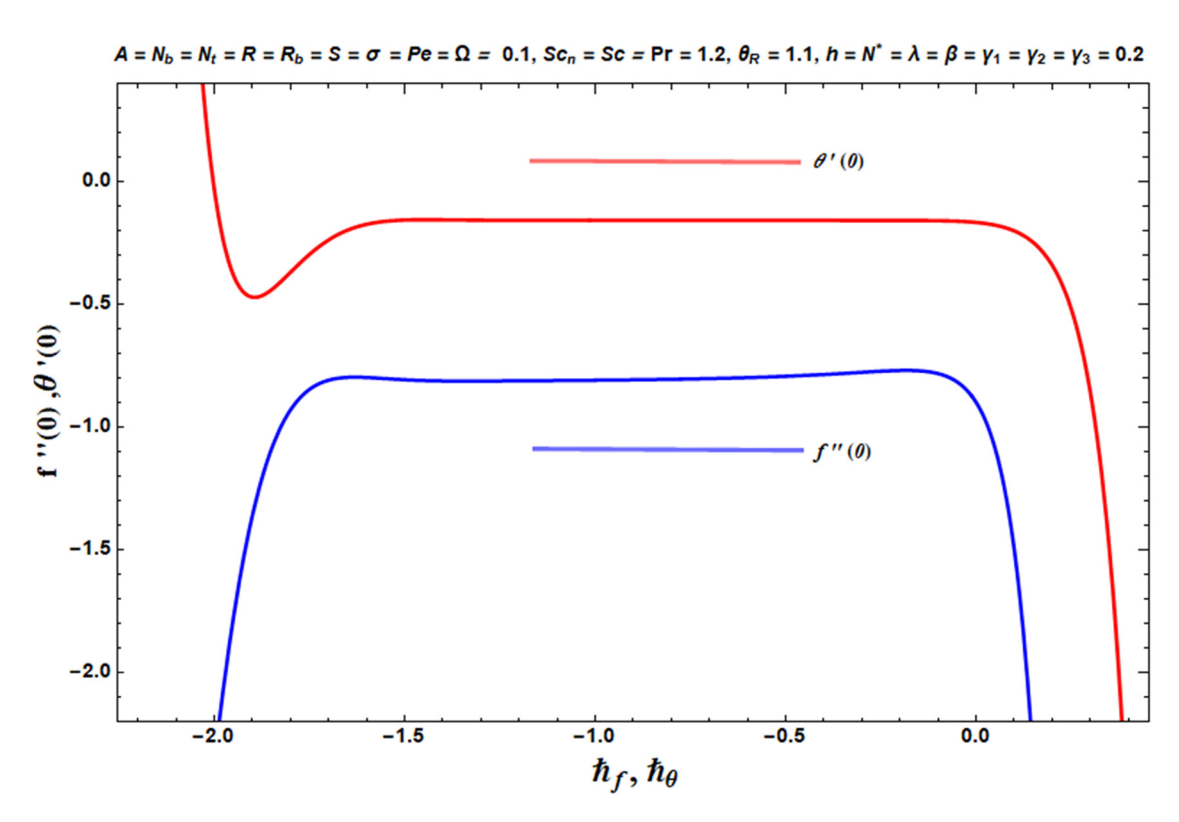


Figure 2: \hbar -curve impact on f''(0) and $\theta'(0)$.

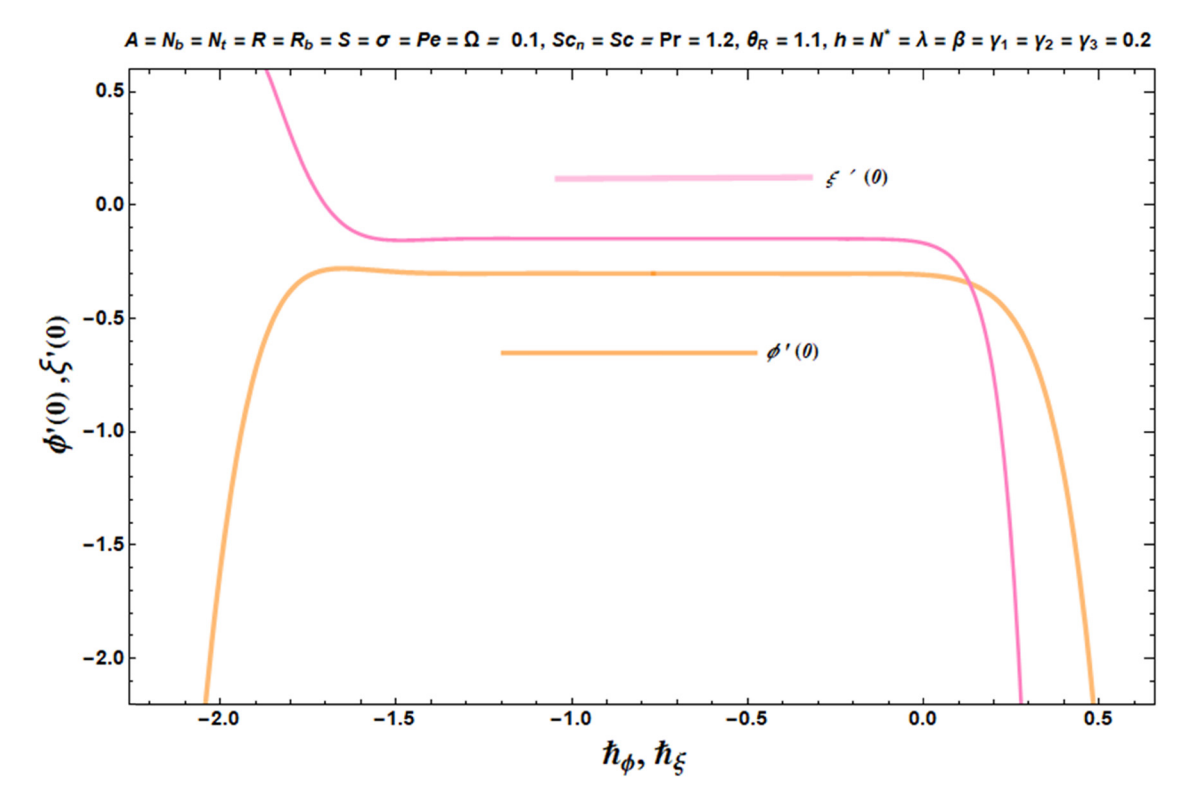


Figure 3: \hbar -curve impact on $\phi'(0)$ and $\xi'(0)$.

 $-1.2 \le h_{\phi} \le -0.2$, and $-1.3 \le h_{\xi} \le -0.2$. Convergence is numerically presented in Table 1.

5 Results and discussions

This segment is presented to clarify the importance of various pertinent parameters like Deborah number β , buoyancy ratio parameter N^* , Prandtl number Pr, radiation parameter R, thermophoresis parameter N_t , heat generation (source)/

Table 1: Assessment of convergence series solutions for the various orders of approximations when $A = N_b = N_t = R = R_b = S = \sigma = Pe = \Omega = 0.1$, $Sc_n = Sc = Pr = 1.2$, $\theta_R = 1.1$, $h = N^* = \lambda = \beta = y_1 = y_2 = y_3 = 0.2$

Order of approximations	<i>f</i> "(0)	$\theta'(0)$	$\phi'(0)$	ξ'(0)	
1	0.80568	0.1611	0.1531	0.1623	
5	0.76479	0.1588	0.1479	0.1611	
10	0.76484	0.1586	0.1477	0.1611	
15	0.79737	0.1584	0.1474	0.1609	
20	0.80194	0.1584	0.1474	0.1609	
25	0.80194	0.1584	0.1474	0.1609	
30	0.80194	0.1584	0.1474	0.1609	
35	0.80194	0.1584	0.1474	0.1609	

(sink) absorption parameter S, temperature ratio parameter θ_R , mixed convection parameter λ , bioconvection Schmidt number Sc_n , bioconvection Rayleigh number Rb, thermal Biot number y_1 , Schmidt number Sc, Brownian motion parameter $N_{\rm b}$, concentration Biot number γ_2 , motile microorganisms Biot number y_3 , bioconvection Peclet number Pe, motile microorganisms concentration difference parameter Ω , and chemical reaction parameter γ on the fluid velocity $f'(\eta)$, temperature $\theta(\eta)$, concentration $\phi(\eta)$, and motile density field $\xi(\eta)$.

5.1 Velocity profile

Figures 4 and 5 illustrate the aspect of β , λ ,Rb, and N^* on velocity $f'(\eta)$. It is noticed from Figure 4 that the Maxwell fluid velocity $f'(\eta)$ displays diminishing behavior with increasing values of β , while it upsurges with increasing λ . The reducing trend in $f'(\eta)$ is noticed for increasing β . Clearly Deborah number encompasses relaxation time and when this factor upsurges, Deborah number becomes greater which engenders resistance in liquid flow and as a result velocity decreases. Moreover, the ratio of acting viscous and buoyant forces in the flow regime is taken into account by the mixed convection parameter λ . Higher values of λ corresponds to a lower viscous force which ultimately accelerates

8 — Shuguang Li et al. DE GRUYTER

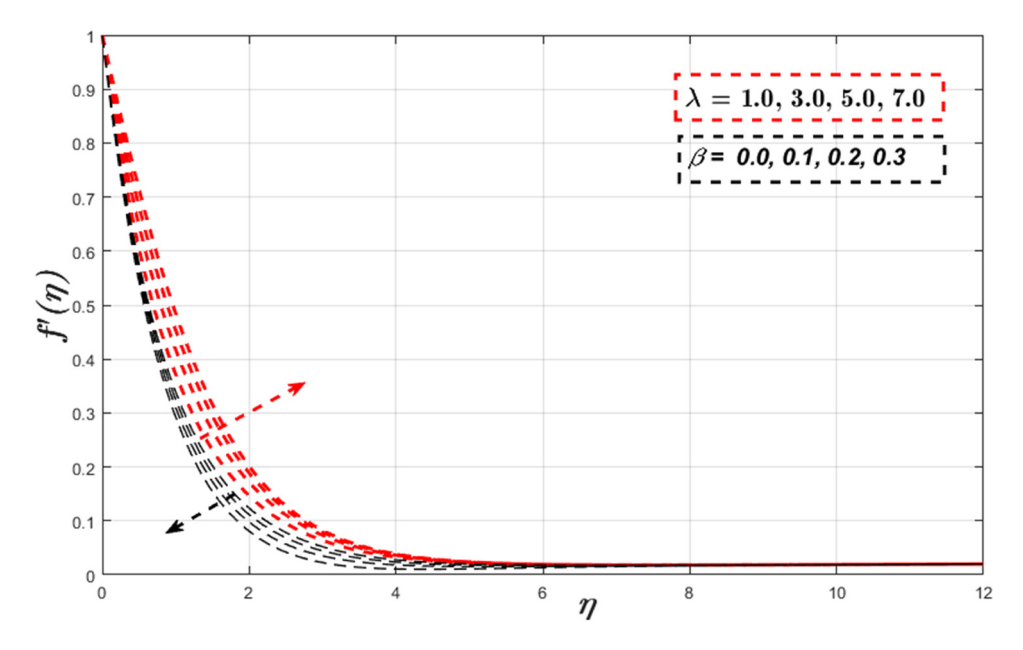


Figure 4: Variation in $f'(\eta)$ via β and λ .

 $f'(\eta)$. Figure 5 depicts the impact of Rb and N^* on the velocity $f'(\eta)$. This figure displays that the increasing values of Rb diminish $f'(\eta)$. This diminishing trend is noticed because Rb and N^* are associated with the buoyant force induced by bioconvection which permits the velocity field to fall.

5.2 Temperature profile

Figures 6–9 display the effect of R, \Pr , γ_1 , N_t , θ_R , S, and N_b on temperature $\theta(\eta)$. The decline in temperature field $\theta(\eta)$ is detected for increasing \Pr (Figure 6). \Pr is a non-dimensional parameter and it is described as the ratio of

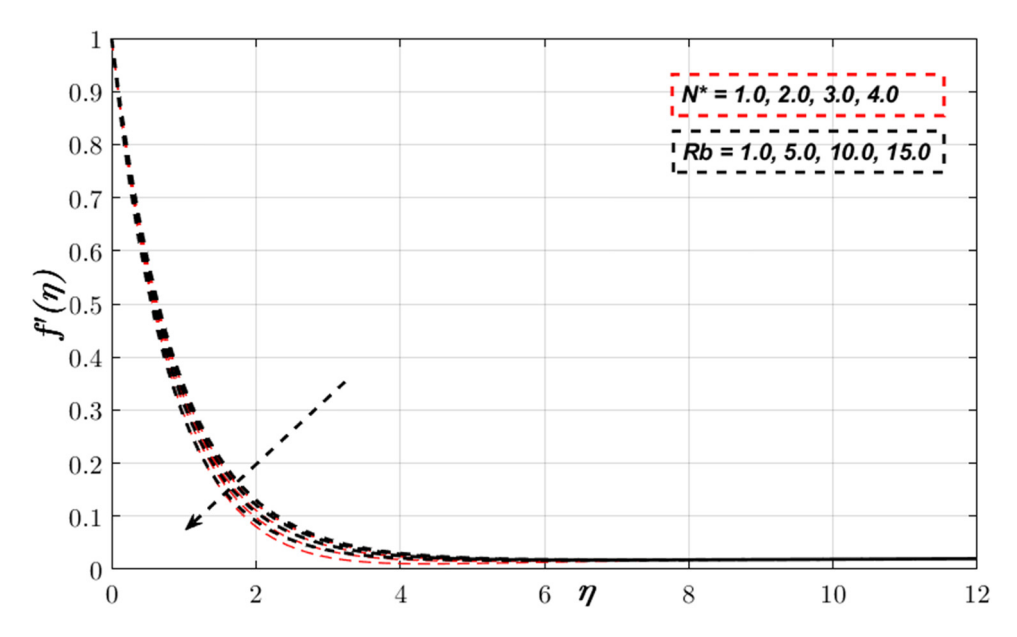


Figure 5: Variation in $f'(\eta)$ via Rb and N*.

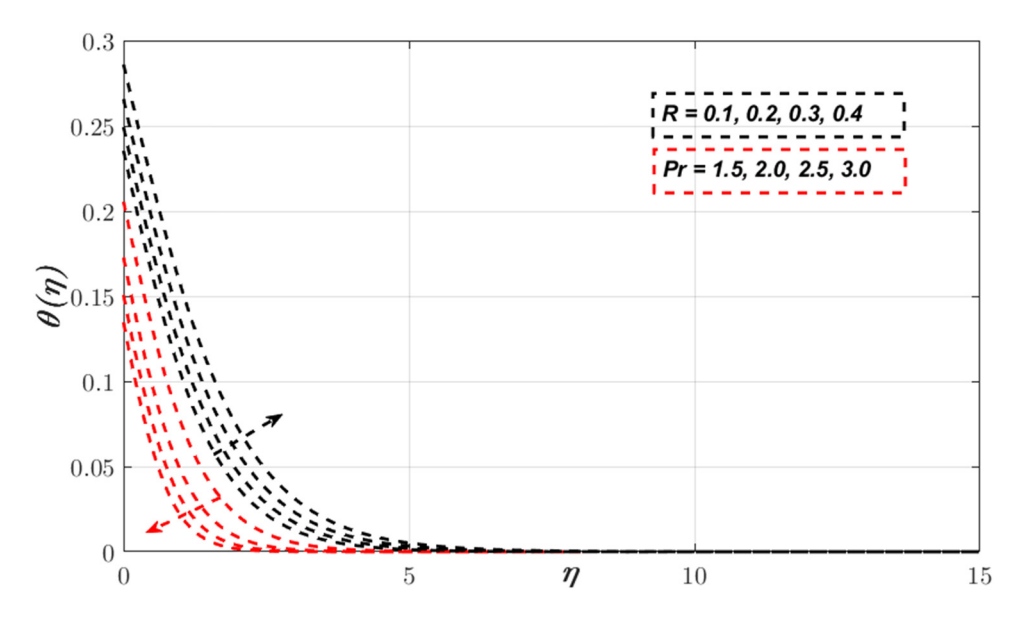


Figure 6: Variation in $\theta(\eta)$ *via* Pr and R.

diffusivities (i.e., momentum and thermal diffusivity). Larger Pr yields lower thermal diffusion due to which $\theta(\eta)$ decays. On the other hand, a rise in R produces $\theta(\eta)$ enhancement. Physically, the transportation of heat with the assistance of liquid elements transpires because of radiation aspect. For that reason, certain heat amount is augmented in flow field. It is evident from Figure 7 that larger values of $N_{\rm b}$ and $N_{\rm t}$ cause an enhancement of temperature field $\theta(\eta)$. The thermophoresis process comprises of relocated fluid particles from hotter to a cooler surface area. In thermophoresis phenomenon, the heated fluid particles shift in the boundary domain from a lower to

higher temperature area, causing the temperature to rise. On the other hand, the Brownian motion diffusion N_b depicts the chaotic fluid particles motion in the regime of flow. With higher values of N_b , the stochastic fluid particles movement upsurges which outcomes an improved temperature field $\theta(\eta)$. Figure 8 is sketched to elucidate on the effects of heat generation (S>0)/absorption (S<0) against $\theta(\eta)$. Here $\theta(\eta)$ is enhanced when S>0 whereas it reduces when S<0. It is investigated that consideration of heat source/sink tends to hasten the liquid movement. Note that S>0 signifies the generation of heat, while S<0 means absorption of heat. Physically the heat source

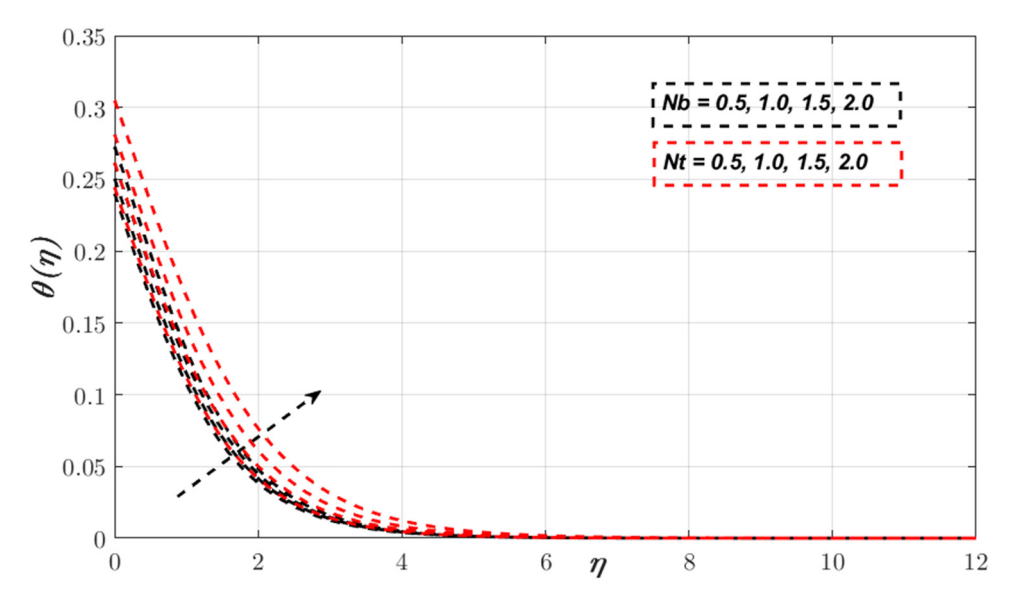


Figure 7: Variation in $\theta(\eta)$ via $N_{\rm b}$ and $N_{\rm t}$.

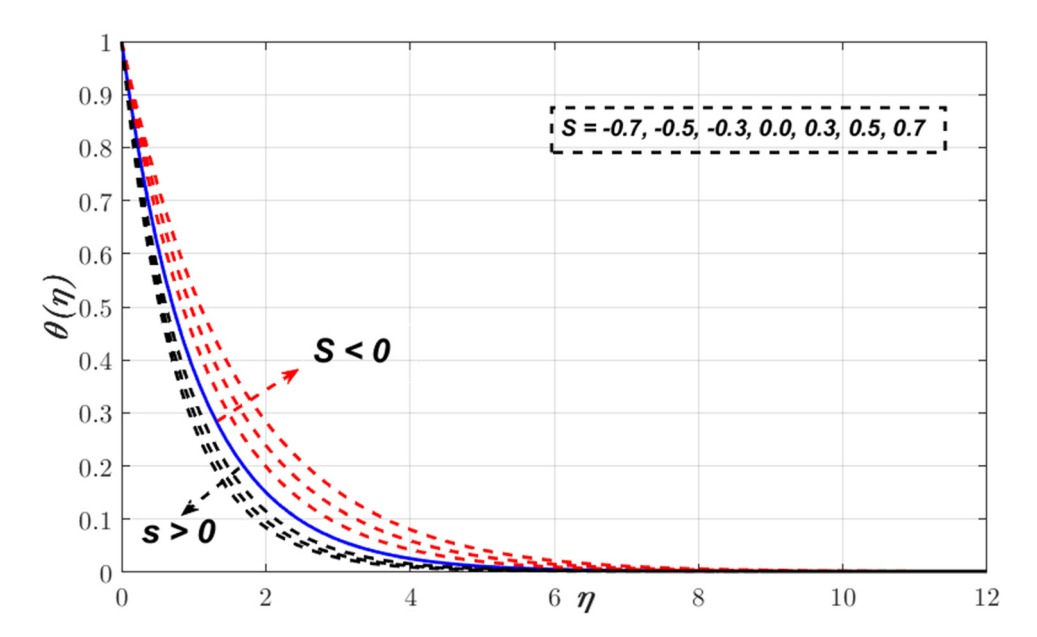


Figure 8: Variation in $\theta(\eta)$ *via S*.

indicates heat generation which upsurges $\theta(\eta)$. Therefore, as heat source variable upsurges, $\theta(\eta)$ increases. On the other hand, $\theta(\eta)$ decays for S < 0. Figure 9 illustrates the consequences of θ_R and γ_1 on temperature $\theta(\eta)$. As expected, larger θ_R and γ_1 corresponds to $\theta(\eta)$ enhancement. Higher θ_R implies a boost in convective liquid temperature, which produces deeper thermal penetration depth into the boundary layer. Heat transfer into flow towards wall is consequently

promoted. Furthermore, when $T_{\rm f}$ surpasses T_{∞} , a larger thermal differential is generated across the boundary layer, which strengthens thermal diffusion from wall towards freestream and results in a rise in $\theta(\eta)$. On the other hand, it is investigated that the temperature field $\theta(\eta)$ escalates with a rise in γ_1 . In fact, increasing γ_1 increases the strength of the coefficient of heat transmission which contributes to accelerating the heat transfer rate.

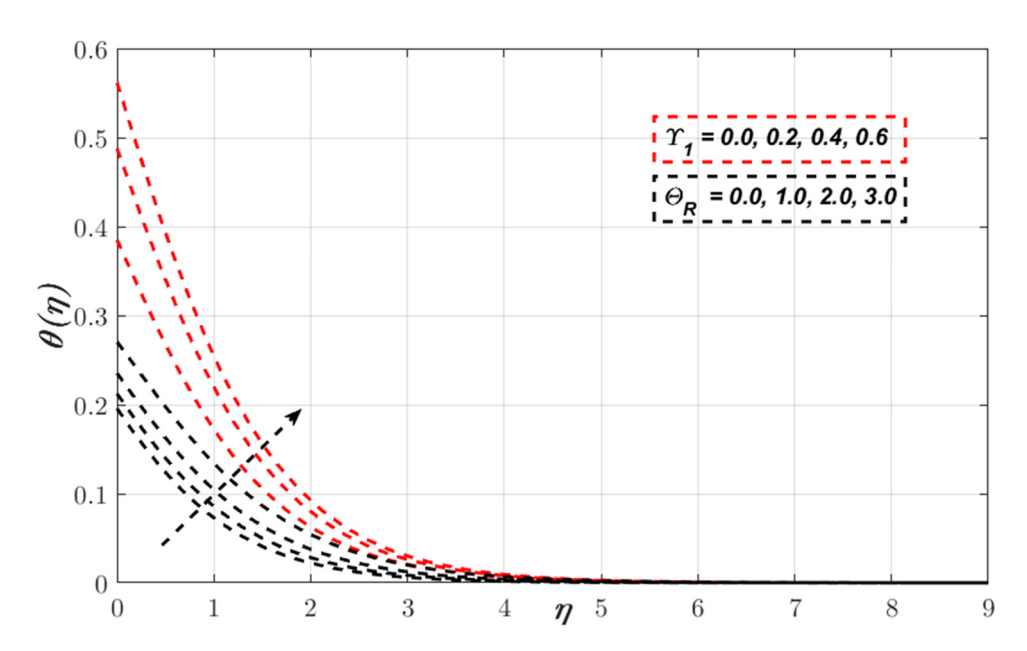


Figure 9: Variation in $\theta(\eta)$ via θ_R and γ_1 .

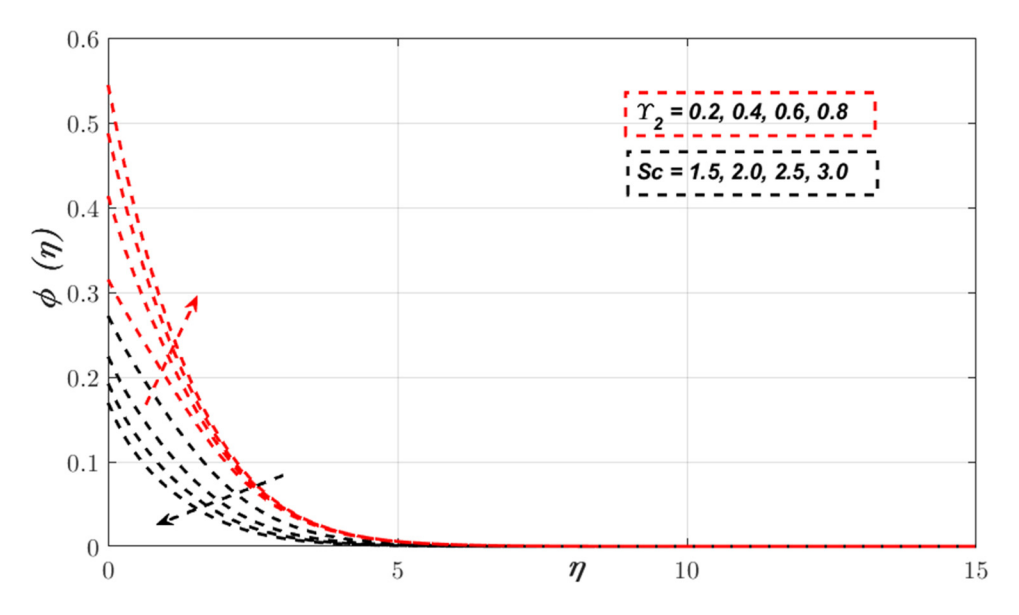


Figure 10: Variation in $\phi(\eta)$ *via* Sc and γ_2 .

5.3 Concentration profile

Figures 10–12 show the impacts of Sc, σ , $N_{\rm t}$, γ_2 , and $N_{\rm b}$ on $\phi(\eta)$. Figure 10 illustrates that an intensification in Sc leads to a decline in volumetric concentration $\phi(\eta)$ of nanoparticles. In fact, Sc has an inverse relationship with Brownian diffusion. Higher values of Sc corresponds to a lower Brownian diffusion which causes a depletion in the nanoparticle's concentration profile $\phi(\eta)$. From this Figure, it is also found that the concentration of nanoparticles $\phi(\eta)$ increases when γ_2 is augmented. The mass transfer quantity increases for higher values of γ_2 which accelerates the

liquid concentration of nanoparticles. Figure 11 portrays the concentration distribution $\phi(\eta)$ for distinct values of $N_{\rm t}$ and $N_{\rm b}$. A diminishing trend is observed when $N_{\rm b}$ is enlarged. The fluid particle collision accelerates for greater values of $N_{\rm b}$. Hence, the concentration of Maxwell nanofluid reduces. On the other hand, contradictory behavior is noticed for $N_{\rm t}$ on the concentration profile $\phi(\eta)$. Physically, the thermophoretic body force elevates which causes the nanoparticles transportation from upper to lower region when $N_{\rm t}$ is increased. Therefore, $\phi(\eta)$ reduces. Figure 12 demonstrates that with higher destructive chemical reaction parameter $\sigma > 0$, concentration $\phi(\eta)$ of nanoparticles

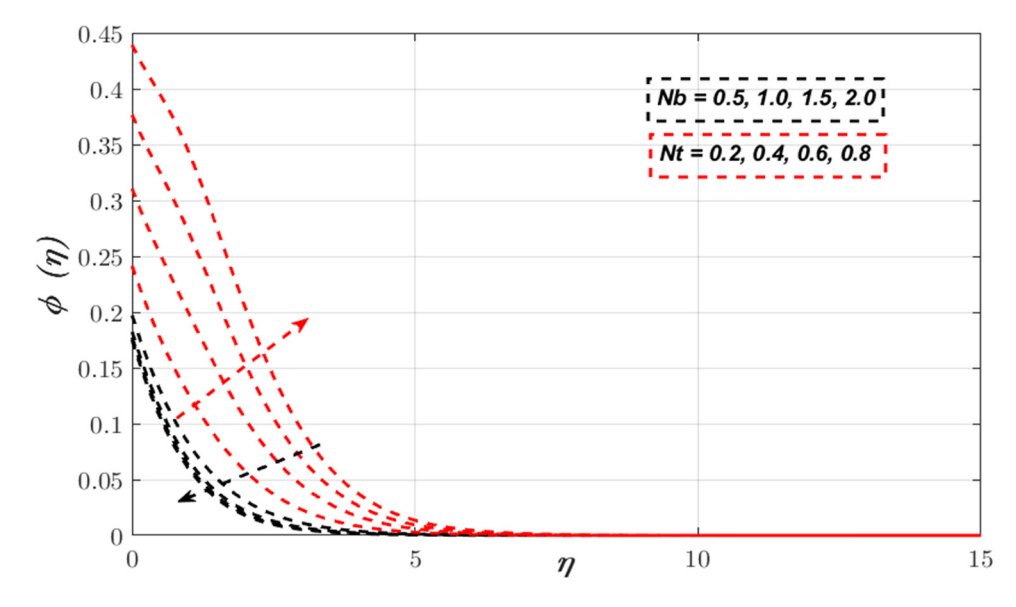


Figure 11: Variation in $\phi(\eta)$ via $N_{\rm b}$ and $N_{\rm t}$.

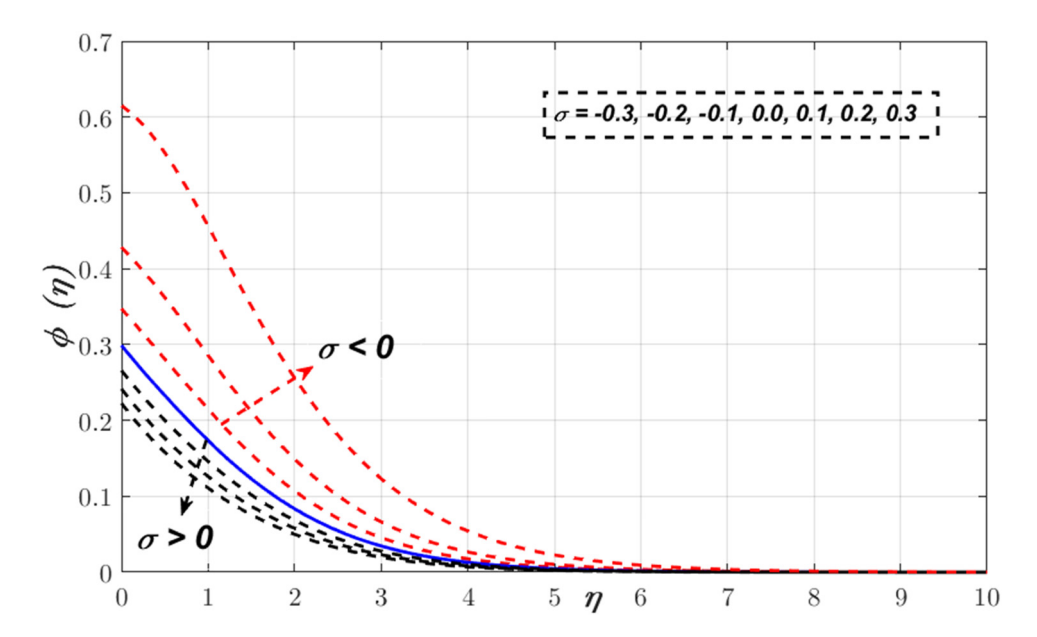


Figure 12: Variation in $\phi(\eta)$ *via* σ .

is suppressed since a larger amount of the nanoparticles are transformed to another species in the domain. The inverse trend is reported with greater generative chemical reaction parameter $\sigma < 0$ for which nanoparticle concentrations are elevated and thickness of solutal boundary layer is also improved.

5.4 Motile microorganism profile

Figures 13 and 14 show the impacts of Sc_n , Pe, γ_3 , and Ω on $\xi(\eta)$. From Figure 13, it is examined that an enhancement in Sc_n causes a decay in the diffusivity of microbes in polymeric liquid, which results in the depletion of the

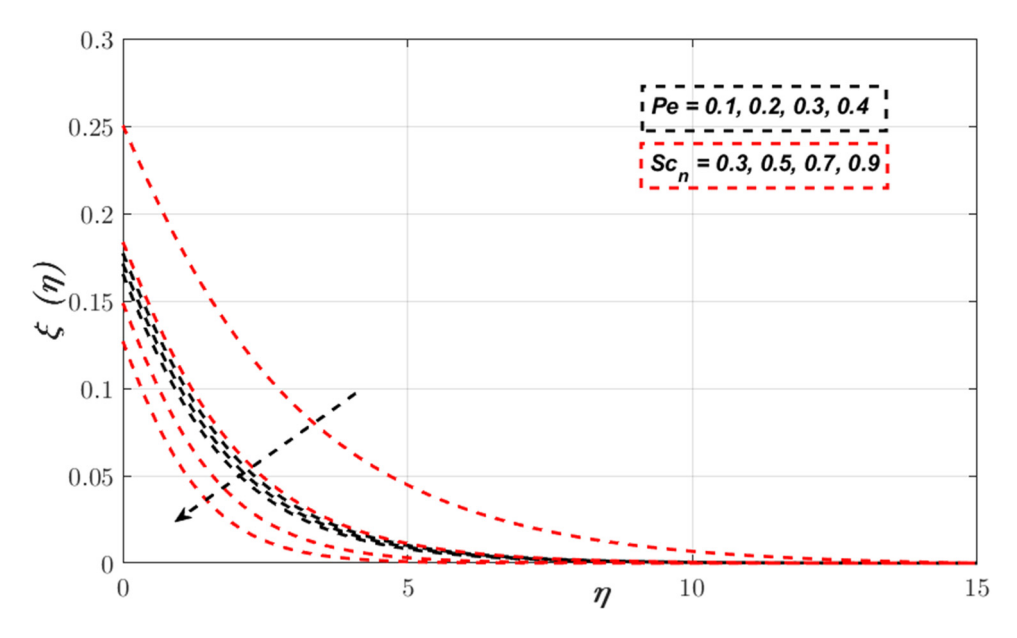


Figure 13: Variation in $\xi(\eta)$ *via* Sc_n and Pe.

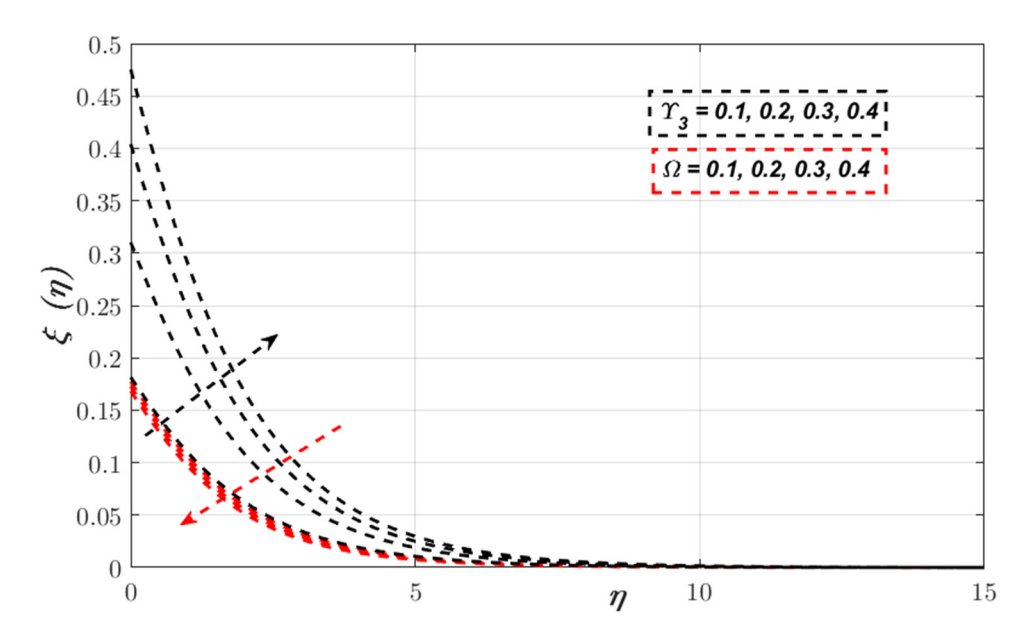


Figure 14: Variation in $\xi(\eta)$ via Ω and γ_3 .

microorganism field. Moreover, Figure 13 displays the aspect of Pe on the microorganism profile $\xi(\eta)$. In fact, Pe is the key parameter to evaluate the microorganisms swimming in the liquid regime. Pe is defined as the ratio of

high cell swimming velocity to microorganism diffusion rate. Diffusion is the mechanism in which a molecule transfers from a region of high concentration to a region of low concentration. It proves the movement of the fluid

Table 2: Numerical values of $Nu_x Re_x^{\frac{1}{2}}$, $Sh_x Re_x^{\frac{1}{2}}$, and $Nn_x Re_x^{1/2}$ for different flow parameters

Rb	N^*	$oldsymbol{ heta}_{ ext{R}}$	N_{t}	$N_{ m b}$	γ_1	y_2	γ_3	$Nu_x Re_x^{\frac{1}{2}}$	$\operatorname{Sh}_{x}\operatorname{Re}_{x}^{\frac{1}{2}}$	$Nn_{\chi}Re_{\chi}^{1/2}$
1.0	0.1	0.1	0.2	0.2	0.2	0.2	0.2	0.1376	0.1469	0.1617
2.0								0.1374	0.1467	0.1616
3.0								0.1372	0.1465	0.1615
0.1	1.0							0.1373	0.1466	0.1616
	2.0							0.1366	0.1462	0.1612
	3.0							0.1357	0.1457	0.1608
	0.1	1.0						0.1524	0.1470	0.1617
		2.0						0.1713	0.1474	0.1618
		3.0						0.3038	0.1488	0.1619
		0.1	0.3					0.1373	0.1386	0.1618
			0.4					0.1368	0.1305	0.1617
			0.5					0.1363	0.1226	0.1616
			0.2	0.3				0.1374	0.1527	0.1619
				0.4				0.1371	0.1555	0.1619
				0.5				0.1367	0.1573	0.1619
				0.2	0.3			0.1844	0.1414	0.1618
					0.4			0.2215	0.1370	0.1619
					0.5			0.2518	0.1335	0.1620
					0.2	0.3		0.1376	0.2022	0.1621
						0.4		0.1373	0.2492	0.1624
						0.5		0.1371	0.2894	0.1626
						0.2	0.3	0.1378	0.1469	0.2214
							0.4	0.1378	0.1469	0.2713
							0.5	0.1378	0.1469	0.3137

particles in the boundary regime. It is noted that microbe's diffusivity is suppressed in the case of an enhancement in Pe. Hence, the microorganism profile $\xi(\eta)$ decreases. Figure 14 describes the influence of Ω on the microorganism field $\xi(\eta)$. It is detected that by enhancing the values of Ω , the concentration of motile microorganisms in ambient liquid is reduced. Also, Figure 14 shows the performance of γ_3 on motile microorganism profile $\xi(\eta)$. It is found that the microorganism distribution $\xi(\eta)$ enlarges when γ_3 is accelerated.

5.5 Physical quantities

The variation in the rates of heat transfer, mass transfer, and microorganism diffusion for flow parameters are presented through Table 2. Here it is found that a diminishing trend in these physical quantities for Rayleigh factor, buoyancy ratio, and thermophoresis parameters is observed, while increasing behavior is observed for the temperature ratio parameter. Furthermore, increasing $N_{\rm b}$ and $\gamma_{\rm 2}$ cause a decrease in heat transfer rate; however increasing behavior is observed for $\gamma_{\rm 1}$. An enhancement is observed in the rate of mass transfer with the growing values of $N_{\rm b}$ and $\gamma_{\rm 2}$. Increasing $\gamma_{\rm 1}$, $\gamma_{\rm 2}$, and $\gamma_{\rm 3}$ cause an elevation in microorganism diffusion rate.

6 Conclusion

The present study captures the thermophoresis body force and Brownian motion aspects in the flow of upper convected Maxwell nanofluid subjected to gyrotactic motile microorganisms. The flow is considered over a porous vertical surface. Nonlinear radiative stagnated flow is formulated considering chemical reaction. The convergence series solutions are obtained through HAM. The key findings are elaborated below:

- The fluid velocity is an increasing function of the mixed convection parameter but opposite outcomes are obtained for the Deborah number.
- 2) The temperature ratio factor yields higher temperature and heat transportation rate.
- Brownian motion and radiation parameters upsurge the nanofluid temperature.
- 4) Concentration profile decays for larger Brownian motion parameter whereas it elevates for larger thermophoresis parameter.
- Larger solutal Biot number and Brownian motion parameter result in the augmentation of the magnitude of local Sherwood number.

- 6) Microorganisms profile declines for larger bioconvection Schmidt number and motile microorganisms difference parameter whereas it improves with stronger Peclet number.
- 7) Magnitude of microorganism diffusion rate boosts directly for larger y_1 , y_2 , and y_3 .

The present communication provides a suitable platform to researchers regarding nanoliquid consideration in higher temperature based nano-polymeric flows subjected to coating processes. However, this research work has overlooked certain effects like activation energy, magnetohydrodynamics, Cattaneo–Christov based dual diffusive flow, entropy generation, and bio-convective flows featuring gyrotactic microorganisms. Such effects will be reported imminently.

Acknowledgments: The authors express their gratitude to Princess Nourah bint Abdulrahman University Researchers Supporting Project number (PNURSP2023R61), Princess Nourah bint Abdulrahman University, Riyadh, Saudi Arabia.

Funding information: Princess Nourah bint Abdulrahman University Researchers Supporting Project number (PNURSP2023R61), Princess Nourah bint Abdulrahman University, Riyadh, Saudi Arabia.

Author contributions: All authors have accepted responsibility for the entire content of this manuscript and approved its submission.

Conflict of interest: The authors state no conflict of interest.

References

- Hayat T, Waqas M, Shehzad SA, Alsaedi A. Mixed convection radiative flow of Maxwell fluid near a stagnation point with convective condition. J Mech. 2013;29:403–9.
- [2] Nadeem S, Akhtar S, Abbas N. Heat transfer of Maxwell base fluid flow of nanomaterial with MHD over a vertical moving surface. Alex Eng J. 2020;59:1847–56.
- [3] Megahed AM. Improvement of heat transfer mechanism through a Maxwell fluid flow over a stretching sheet embedded in a porous medium and convectively heated. Math Comput Simul. 2021:187:97–109.
- [4] Madkhali HA, Haneef M, El-Shafay AS, Alharbi SO, Nawaz M. Mixed convective transport in Maxwell hybrid nano-fluid under generalized Fourier and Fick laws. Int Commun Heat Mass Transf. 2022;130:105714.
- [5] Waqas M. Chemical reaction impact in dual diffusive non-Newtonian liquid featuring variable fluid thermo-solutal attributes. Chem Phys Lett. 2022;802:139661.

- [6] Sankar M, Swamy HAK, Do Y, Altmeyer S. Thermal effects of nonuniform heating in a nanofluid-filled annulus: Buoyant transport versus entropy generation. Heat Transf Asian Res. 2021;51:1062-91. doi: 10.1002/htj.22342.
- Elayarani M, Shanmugapriya M, Kumar PS. Intensification of heat and mass transfer process in MHD carreau nanofluid flow containing gyrotactic microorganisms. Chem Eng Process - Process Intensif. 2021:160:108299.
- Zaimi K, Ishak A, Pop I. Stagnation-point flow toward streching/ shrinking sheet in a nanofluid containing both nanoparticles and gyrotactic microorganisms. ASME J Heat Transf. 2014;136:041705.
- Xu H, Pop I. Fully developed mixed convection flow in a horizontal channel filled by a nanofluid containing both nanoparticles and avrotactic microorganisms. Eur I Mech - B/Fluids. 2014:46:37-45.
- [10] Waqas M, Hayat T, Shehzad SA, Alsaedi A. Transport of magnetohydrodynamic nanomaterial in a stratified medium considering gyrotactic microorganisms. Phys B: Condens Matter. 2018;529:33-40.
- [11] Zohra FT, Uddin MJ, Ismail AIM. Magnetohydrodynamic bio-nanoconvective Naiver slip flow of micropolar fluid in a stretchable horizontal channel. Heat Transf Asian Res. 2019;48:3636-56. doi: 10.1002/htj.21560.
- Anjum N, Khan WA, Azam M, Ali M, Waqas M, Hussain I. [12] Significance of bioconvection analysis for thermally stratified 3D cross nanofluid flow with gyrotactic microorganisms and activation energy aspects. Therm Sci Eng Prog. 2023;38:101596. doi: 10.1016/j. tsep.2022.101596.
- Khan AA, Arshad A, Ellahi R, Sait SM. Heat transmission in Darcy-[13] Forchheimer flow of Sutterby nanofluid containing gyrotactic microorganisms. Int J Numer Methods Heat & Fluid Flow. 2023;33:135-52.
- [14] Ward T, Jensen O, Power H, Riley D. High-Rayleigh-number convection of a reactive solute in a porous medium. I Fluid Mech. 2014:760:95-126.
- [15] Islam AW, Lashgari HR, Sephernoori K. Double diffusive natural convection of CO₂ in a brine saturated geothermal reservoir: Study of non-modal growth of perturbations and heterogeneity effects. Geothermics. 2014;51:325-36.
- [16] Rashidi MM, Ferdows M, Uddin MJ, Anwar Bég O, Rahimzadeh N. Group theory and differential transform analysis of mixed convective heat and mass transfer from a horizontal surface with chemical reaction effects. Chem Eng Commun. 2012;199:1012-43.
- [17] Xin F, Li XF, Xu M, Huai XL, Cai J, Guo ZX. Simulation of gas exothermic chemical reaction in porous media reactor with lattice Boltzmann method. J Therm Sci. 2013;22:42-7.

- [18] Reddy NN, Rao VR, Reddy BR. Chemical reaction impact on MHD natural convection flow through porous medium past an exponentially stretching sheet in presence of heat source/sink and viscous dissipation. Case Stud Therm Eng. 2021;25:100879.
- [19] Hussain M, Ranjha QA, Anwar MS, Jahan S, Ali A. Eyring-Powell model flow near a convectively heated porous wedge with chemical reaction effects. J Taiwan Inst Chem Eng. 2022;139:104510.
- Chu YM, Abbasi A, Al-Khaled K, Faroog W, Khan SU, Khan MI, et al. Mathematical modeling and computational outcomes for the thermal oblique stagnation point investigation for non-uniform heat source and nonlinear chemical reactive flow of Maxwell nanofluid. Case Stud Therm Eng. 2023;41:102626.
- [21] Bhatti MM, Oztop HF, Ellahi R. Study of the magnetized hybrid nanofluid flow through a flat elastic surface with applications in solar energy. Materials. 2022;15:7507.
- Bhatti MM, Ellahi R. Numerical investigation of non-Darcian nanofluid [22] flow across a stretchy elastic medium with velocity and thermal slips. Numer Heat Transfer, Part B: Fundamentals. 2023;83:323-43.
- Zubair M, Wagas M, Nasir M, Bafakeeh OT, Ameen HFM, Galal AM. A theoretical study on partial slip impact in radiative-hydromagnetic liquid configured by extending surface. Int J Mod Phys B. 2022;37:2350074.
- Li S, Khan MI, Alzahrani F, Eldin SM. Heat and mass transport analysis in radiative time dependent flow in the presence of Ohmic heating and chemical reaction, viscous dissipation: An entropy modeling. Case Stud Therm Eng. 2023;42:102722.
- [25] Liao S. Beyond Perturbation: Introduction to the Homotopy Analysis Method. New York: Chapman and Hall/CRC; 2003.
- [26] Hayat T, Sadiq MA. Darcy-Forchheimer flow of magneto Maxwell liquid bounded by convectively heated sheet. Results Phys. 2016;6:884-90.
- Pasha AA, Irshad K, Algarni S, Algahtani T, Wagas M. Analysis of tangent-hyperbolic rheological model considering nonlinear mixed convection, Joule heating and Soret-Dufour aspects from a stretchable convective stratified surface. Int Commun Heat Mass Transf. 2023:140:106519.
- [28] Li S, Puneeth V, Saeed AM, Singhal A, Al-Yarimi FAM, Khan MI, et al. Analysis of the Thomson and Troian velocity slip for the flow of ternary nanofluid past a stretching sheet. Sci Rep. 2023;13:2340.
- [29] Haupt K, Mosbach K. Molecularly Imprinted Polymers and Their Use in Biomimetic Sensors. Chem Rev. 2000;100:2495-504.
- [30] Stolov AA, Wrubel JA, Simoff DA. Thermal stability of specialty optical fiber coatings. J Therm Anal Calorim. 2016;124:1411-23.
- Rivero PJ, Goicoechea J, Arregui FJ, Optical fiber sensors based on polymeric sensitive coatings. Polymers. 2018;10:280.